Preprints of the 21st IFAC World Congress (Virtual)
Berlin, Germany, July 12-17, 2020

Information and Collaboration Levels in Vehicular Strings: A Comparative Study ⋆

R. Austin Dollar * **Antonio Sciarretta** ** **Ardalan Vahidi** ***

* *IFP Energies nouvelles (visitor), Rueil-Malmaison, France (e-mail: rdollar@clemson.edu).*
** *IFP Energies nouvelles, Rueil-Malmaison, France (e-mail: antonio.sciarretta@ifp.fr)*
*** *Clemson University, Clemson, SC 29634 USA (e-mail: avahidi@clemson.edu).*

Abstract: The potential safety, productivity, and energy benefits of automated vehicles have driven a surge of research interest in their algorithms. Even within single-lane driving, control engineers now have a profusion of approaches available to them. Algorithm classes include classical controllers, receding horizon controllers, and constrained eco-driving formulae based on Pontryagin's Minimum Principle. Differing connectivity architectures and collaboration levels further differentiate algorithms from one another. This study evaluated six controllers in two drive cycle-based scenarios using an electric powertrain model for energy analysis. Individual-vehicle and string performance were examined, including string stability and length. Algorithms with greater access to information generally performed best. Although collaboration affected energy use only slightly, it made a greater impact on string length.

Keywords: Multi-vehicle systems, trajectory and path planning, nonlinear and optimal automotive control.

1. INTRODUCTION

Even at lower autonomy levels, longitudinal vehicle controllers can reduce driving effort. These systems could also help dissipate traffic jams although, as Gunter et al. (2019) showed, this does not always materialize in production. The designs vary in their structure, control objective, and hardware technology. While several literature reviews have compared available algorithms over the years (Vahidi and Eskandarian (2003), Xiao and Gao (2010), Sciarretta and Vahidi (2019)), the individual data sources typically evaluate designs in different scenarios. Because algorithm performance depends on the scenario, this makes a scientific comparison difficult or impossible to extract.

Automated car-following has become somewhat common commercially. It tracks speed or headway relative to the front vehicle. Some explicit human driver models accomplish this as shown in Milanés and Shladover (2014). Classical adaptive cruise control (ACC) has proven suitable (Ntousakis et al. (2015)), but researchers including Dollar and Vahidi (2018b) and Kim et al. (2019) have proposed optimal control for improved performance. The associated preview's shorter-term validity makes receding horizon control (RHC) a natural choice. RHC also integrates elegantly with connectivity or data-driven prediction models. Alternatively, He et al. (2019) proposed explicit feedback control using multiple connected vehicles' speeds.

⋆ This material is based upon research supported by the Chateaubriand Fellowship of the Office for Science & Technology of the Embassy of France in the United States in addition to research supported by the U.S. Department of Energy Vehicle Technologies Office (Project No. DE-EE0008232).

Another approach referred to as eco-driving seeks to optimize a vehicle's speed trajectory between two boundary points. This is typically cast as an open-loop or shrinking-horizon (Paredes et al. (2019)) problem and solved using dynamic programming (DP) or Pontryagin's Minimum Principle (PMP). Such solutions have typically not included traffic as exemplified in Kim et al. (2010) and Han et al. (2019), focusing instead on powertrain awareness. However, position-constrained results like the one found in Han et al. (2018) could potentially fill the role of ACC.

One contribution of this study is a scorecard based on common scenarios and featuring several different algorithms, some of which have fundamentally different designs. String stability is examined along with overall performance considering both electric vehicle (EV) energy efficiency and string compactness. While the decentralized hierarchical controller of Section 6.2 is a special case of the multi-lane algorithm of Dollar and Vahidi (2020) and its centralized form is similarly related to Dollar et al. (2020), the cooperative variant in Section 6.4 is new. Furthermore, this is the first simulation assessment of Section 5's position-constrained shrinking horizon algorithm in a string.

Section 3 begins the algorithm discussion with classical ACC. Then, Section 4 reviews EV eco-driving before Sections 5 and 6 apply the results to shrinking horizon and hierarchical controllers. Section 7 reviews the simulation scenarios and methods and Section 8 presents the results. Finally, Section 9 reflects on the algorithms' usefulness and identifies opportunities for further development.

2. PROBLEM STATEMENT

2.1 Point-to-Point Car Following

This paper deals with the problem of propelling a vehicle from one fixed point to another while following another preceding vehicle (PV), which may be part of a sequence of vehicles called a string. The ego vehicle senses the position and speed of the PV and, in connected designs, may also access the PV's current acceleration or even future intentions. The eco-driving or ACC controller commands acceleration, leaving powertrain and brake control to a lower-level module.

2.2 Plant Model

The simulated system dynamics follow the approach of Dollar and Vahidi (2018b). Equation (1) shows the linear model with position s, velocity v, and acceleration a composing the state vector x. The acceleration lags its command u with time constant $\tau_a = 0.275\,\mathrm{s}$.

$$\frac{d}{dt}\begin{bmatrix} s \\ v \\ a \end{bmatrix} = \underbrace{\begin{bmatrix} 0 & 1 & 0 \\ 0 & 0 & 1 \\ 0 & 0 & -\frac{1}{\tau_a} \end{bmatrix}}_{A} \begin{bmatrix} s \\ v \\ a \end{bmatrix} + \underbrace{\begin{bmatrix} 0 \\ 0 \\ \frac{1}{\tau_a} \end{bmatrix}}_{B} u \tag{1}$$

Unlike Dollar and Vahidi (2018b) where separate time constants represent the engine and brake lags, this electric vehicle (EV)-oriented paper uses a single global time constant. The longer engine time constant previously represented phenomena like turbocharger lag that can have rise time on the order of seconds (Bemporad et al. (2018)). EVs lack such fluid-dynamic mechanisms.

The model (1) is relatively simple. In the authors' experimental experience however, algorithm concepts developed using (1) can still improve efficiency on a real vehicle given a well-tuned acceleration controller.

3. CLASSICAL ADAPTIVE CRUISE CONTROL

Classical ACC uses current positions and velocities of the ego and surrounding vehicles in explicit formulae to produce a control input. This includes the controller described and evaluated by Ntousakis et al. (2015), which is reviewed here. Parameters include the desired speed v_d and time headway T. A proportional speed controller transitions to a proportional-derivative gap controller when appropriate. Even in gap control mode, the ACC acceleration command u_c does not exceed the one from speed control. In (2), d denotes the current gap, d_d the desired gap, v_e and d_e the speed and gap errors, and a_{sc} the acceleration from speed control. As in all algorithms, the acceleration command may not exceed the vehicle's maximum acceleration $\overline{u}(v)$. The following control law is recomputed at each timestep k, although the argument is dropped.

$$v_e = v - v_d \tag{2a}$$

$$a_{sc} = \max\left\{\min\left\{-0.4v_e,\ 2\right\},\ -2\right\} \tag{2b}$$

$$d_e = d - d_d, \quad d_d = Tv \tag{2c}$$

$$u_c = \begin{cases} a_{sc} & \text{speed control} \\ \max\left\{\min\left\{\dot{d} + 0.25d_e,\ a_{sc}\right\},\ -2\right\} & \text{gap control} \end{cases} \tag{2d}$$

$$u = \min\left\{u_c, \overline{u}(v)\right\} \tag{2e}$$

Mode transitions between speed and gap control depend on current gap with hysteresis. If gap exceeds 120 m, the system switches from gap to speed control; if gap falls below 100 m, the opposite transition takes place.

All parameters in (2) come from Shladover et al. (2012), which states that the speed gain 0.4 yields a "typical" and "gentle" response. Time headway T has a major impact on ACC performance; specifically, it controls the trade-off between string stability and compactness. Therefore, Section 8 includes results for two different values of T. Ntousakis et al. (2015) documents the traffic flow effects of T in Aimsun simulations.

4. ECO-DRIVING OF ELECTRIC VEHICLES

This section reviews minimum-energy eco-driving of EVs, leading to the parabolic speed profile employed in the optimal control approaches of Sections 5 and 6. The provided solutions follow Sciarretta and Vahidi (2019).

4.1 Basic Optimal Control Problem and Solution

To minimize cumulative energy consumption, the objective of optimal control problem (OCP) (3) integrates a battery output power model with constant coefficients p_0 and p_1 over future time τ until the final time τ_f. The result approximates the total energy discharged from the battery. Both power and regenerative modes use the same integrand in J; a negative value for the first term corresponds to regenerative braking. The second term with coefficient p_1 accounts for resistance losses that occur in both power and regenerative modes. Thus (3) accounts for the major EV energy flows, albeit with less detail than the energy evaluation model of Section 7.2. Constraints fix initial and final conditions 0 and s_f on position and v_i and v_f on velocity.

$$\begin{aligned} \min\ J = & \int_0^{\tau_f} \left[p_0 u(\tau)\, v(\tau) + p_1 u^2(\tau)\right] d\tau \\ \text{s.t.}\quad & s(0) = 0 \\ & v(0) = v_i \\ & s(\tau_f) = s_f \\ & v(\tau_f) = v_f \end{aligned} \tag{3}$$

In the absence of further active constraints and assuming constant resistive force, (3) results in speed as the following parabolic function of time.

$$\begin{aligned} v(\tau) = & v_i + \left(\frac{-4v_i}{\tau_f} - \frac{2v_f}{\tau_f} + \frac{6s_f}{\tau_f^2}\right)\tau \\ & + \left(\frac{3v_i}{\tau_f^2} - \frac{6s_f}{\tau_f^3} + \frac{3v_f}{\tau_f^2}\right)\tau^2, \quad \tau \in [0,\ \tau_f) \end{aligned} \tag{4}$$

4.2 Position Constraints

Sciarretta and Vahidi (2019) also provide the implicit solution for (3) after adding a position constraint that assumes a known constant PV acceleration a_p from initial PV relative position $s_{p,0}$ and speed $v_{p,0}$. The PV acceleration can either be obtained from connectivity where the PV need not be automated, or estimated with lag. This study does not consider such lag and is more representative of the connected case.

$$s(\tau) \leq s_{p,0} + v_{p,0}\tau + \frac{1}{2}a_p\tau^2, \quad \tau \in [0,\ \tau_f] \tag{5}$$

The following equations describe the solution, where the ego begins at velocity v_i and ends at velocity $v_f = 0$.

$$\begin{aligned} v(\tau) =& v_i + \left(a_p + \frac{4(v_{p,0} - v_i)}{\tau_1} + \frac{6s_{p,0}}{\tau_1^2}\right)\tau \\ &- \left(\frac{6s_{p,0}}{\tau_1^3} + \frac{3(v_{p,0} - v_i)}{\tau_1^2}\right)\tau^2, \quad \tau \in [0,\ \tau_1) \end{aligned} \tag{6}$$

Equation (6) contains the unknown contact time τ_1 when the ego vehicle reaches the position constraint. This time solves the following cubic equation.

$$\begin{aligned} &(v_i - v_f + a_p\tau_f)\,\tau_1^3 \\ &+ \left(4v_{p,0}\tau_f + v_f\tau_f - 2v_i\tau_f + \frac{a_p\tau_f^2}{2} - 3s_f\right)\tau_1^2 \\ &+ \left(6s_{p,0}\tau_f + v_i\tau_f^2 - v_{p,0}\tau_f^2\right)\tau_1 - 3s_{p,0}\tau_f^2 = 0 \end{aligned} \tag{7}$$

4.3 Speed Constraints

The substitution of a constraint to maximum speed $\overline{v}$ instead of position is also quite tractable and yields the following explicit solution as reported by Sciarretta and Vahidi (2019). The times τ_1 and τ_2 in (8) now refer to the boundaries of the interval where $v = \overline{v}$.

$$v(\tau) = \begin{cases} v_i + \frac{2(\overline{v}-v_i)}{\tau_1}\tau - \frac{\overline{v}-v_i}{\tau_1^2}\tau^2 & \tau \in [0,\ \tau_1) \\ \overline{v} & \tau \in [\tau_1,\ \tau_2] \\ v_f + \dfrac{2(\overline{v} - v_f)}{\tau_f - \tau_2}(\tau_f - \tau) - \dfrac{\overline{v} - v_f}{\tau_f - \tau_2}(\tau_f - \tau)^2 & \tau \in [\tau_2,\ \tau_f) \end{cases} \tag{8a}$$

$$\tau_2 = \tau_f - \tau_1\sqrt{\frac{\overline{v} - v_f}{\overline{v} - v_i}} \tag{8b}$$

$$\tau_1 = \frac{3(\overline{v}\tau_f - s_f)\sqrt{\overline{v} - v_i}}{(\overline{v} - v_f)^{\frac{3}{2}} + (\overline{v} - v_i)^{\frac{3}{2}}} \tag{8c}$$

4.4 Free Final Time

So far, this section has considered the final time as fixed. Now, the final time is varied to minimize the total energy E_b consumed in the basic parabolic speed trajectory from Section 4.1. Sciarretta and Vahidi (2019) provide the following formula for E_b, where h denotes the resistive acceleration, m_v the vehicle mass, and b a combined modeling constant that cancels from the solution.

$$\begin{aligned} E_b =& m_v h s_f + m_v\frac{v_f^2 - v_i^2}{2} + bh^2\tau_f + 2bh(v_f - v_i) \\ &+ 4b\left(\frac{3s_f^2}{\tau_f^3} - \frac{3s_f(v_i + v_f)}{\tau_f^2} + \frac{v_i^2 + v_iv_f + v_f^2}{\tau_f}\right) \end{aligned} \tag{9}$$

Applying $v_f = 0$, scaling by the positive constant b, and dropping terms not depending on τ_f yields the following simplified energy $\tilde{E}_b$.

$$\tilde{E}_b = h^2\tau_f + 4\left(\frac{3s_f^2}{\tau_f^3} - \frac{3s_fv_i}{\tau_f^2} + \frac{v_i^2}{\tau_f}\right) \tag{10}$$

The stationary points of (10), which solve (12), are candidates for the optimal τ_f along with any bounds. Equation (10) gives the simplified energies for each candidate and the minimum follows by direct enumeration.

$$\frac{\partial\tilde{E}_b}{\partial\tau_f} = h^2 - 4v_i^2\tau_f^{-2} + 24s_fv_i\tau_f^{-3} - 36s_f^2\tau_f^{-4} = 0 \tag{11}$$

$$h^2\tau_f^4 - 4v_i^2\tau_f^2 + 24s_fv_i\tau_f - 36s_f^2 = 0 \tag{12}$$

5. SHRINKING HORIZON ECO-DRIVING

With the addition of a few features, Sections 4.1 and 4.2 become the basis of a longitudinal controller referred to here as Position-Constrained Shrinking Horizon Control (PCSHC). The shrinking horizon scheme is described next, followed by the extraction of the control input from Section 4's results. Then, Sections 5.3 and 5.4 address feasibility and close proximity to the PV, respectively.

5.1 The Shrinking Horizon Concept

This controller operates in closed-loop. After solving the appropriate OCP from Section 4 at step k, the current input is applied and the process repeated at step $k+1$ with a one-step shorter horizon. In other words, shrinking horizon control repeatedly applies Section 4 in a reference frame centered at the current time and ego position. The following equations set the OCP's speed inputs.

$$v_i = v(k), \quad v_f = 0 \tag{13}$$

Equation (14) shifts the reference frame to match Section 4. By default, Section 4's $s_f = s_{fd}$ and $\tau_f = \tau_{fd}$, although the module described in Section 5.3 may alter them. Let t denote global time, while t_{fd} and $\overline{s}_{fd}$ denote the goal time and position in the global frame.

$$s_{fd} = \overline{s}_{fd} - s(k), \quad \tau_{fd} = t_{fd} - t(k) \tag{14}$$

5.2 Extracting the Optimal Control Input

Assume that the position-constrained OCP described by (3) and (5) is feasible and the initial gap exceeds its specified minimum. First, coefficients of the basic parabolic trajectory of Section 4.1 are determined. If the resulting position trajectory does not intersect that of the PV, (4) is differentiated with respect to time and evaluated at $\tau = 0$ to obtain the optimal control input u_o. The argument k is dropped here as in Section 3.

$$u_o = \frac{-4v_i}{\tau_f} - \frac{2v_f}{\tau_f} + \frac{6s_f}{\tau_f^2} \tag{15}$$

If contact would occur, u_o is similarly obtained from (6).

$$u_o = a_p + \frac{4(v_{p,0} - v_i)}{\tau_1} + \frac{6s_{p,0}}{\tau_1^2} \tag{16}$$

5.3 Feasibility

The position constraint can render OCP (3) infeasible. In such cases, an adjustment to the desired boundary conditions s_{fd} and τ_{fd} results in a feasible problem for actual boundary conditions s_f and τ_f. The adjustment considers the following two infeasibility cases.

Preceding Vehicle Stops at an Earlier Position In this case, the constant acceleration a_p leads to the PV stopping at a position less than $\overline{s}_{fd}$ and blocking the ego from reaching $\overline{s}_{fd}$. s_f is then adjusted to the stopped PV position and the minimum-energy problem is solved with τ_f free. This attempts to avoid waste of energy before the PV changes its acceleration.

The procedure of Section 4.4 with bounds

$$\frac{-v_{p,0}}{a_p} \leq \tau_f \leq \min\left\{\tau_{fd},\ \frac{3s_f}{v_i}\right\} \tag{17}$$

yields the new τ_f. The lower bound $\frac{-v_{p,0}}{a_p}$ prohibits arrival at s_f before the PV and, as Sciarretta and Vahidi (2019) show, the upper bound $\frac{3s_f}{v_i}$ prevents $v < 0$ in the solution.

Preceding Vehicle Reaches the Final Position Too Late Even when the preceding vehicle reaches the final position, it may not do so soon enough for the ego vehicle to meet its target time t_{fd}. In such cases, the ego vehicle adjusts τ_f to the time until the position constraint reaches s_{fd}. This time solves the following quadratic equation with $\tau_f > \tau_{fd}$.

$$0 = \frac{1}{2}a_p\tau_f^2 + v_{p,0}\tau_f + s_{p,0} - s_{fd} \tag{18}$$

5.4 Control Under Constraint Violation

The solution of (6) is not defined when a disturbance like prediction or modeling error results in a small violation of the gap constraint. In this case, the event at τ_1 has already occurred and u_o nominally results from the unconstrained parabolic speed profile i.e. (15). However, the control input should always reduce the constraint violation in this case for safety. Therefore, a modified ACC limits the acceleration command under a gap constraint violation ϵ_d. The gain on ϵ_d is borrowed from the gap gain in (2d).

$$u_c = \min\left\{a_p + \dot{d} - 0.25\epsilon_d,\ a_p\right\} \tag{19a}$$

$$u = \min\left\{u_c, u_o, \overline{u}(v)\right\} \tag{19b}$$

6. HIERARCHICAL CONTROLLERS

In reality, the preceding vehicle generally does not proceed with constant acceleration a_p. Some algorithms like Dollar and Vahidi (2018b) seek improved control by anticipating more complex PV trajectories. In a connected environment, this information can come from the PV albeit with limited time horizon. This characteristic of the problem makes RHC attractive. Relative to PMP-based shrinking-horizon control, however, RHC typically loses the capability to plan the speed profile for long-term energy minimization considering the trip's duration and final position. Dollar and Vahidi (2020) addressed this problem in a multi-lane environment by providing a shrinking-horizon reference for RHC. This section applies a similar hierarchical approach on a single lane to assess its usefulness in car-following situations.

Various strategies for reaching a multi-agent solution are described and evaluated in the following subsections. First, the vehicles could solve their individual problems sequentially based on their PVs' optimal position trajectories. Alternatively, one lead vehicle could centrally optimize a string of connected automated vehicles (CAVs) and send commands to the others. A third approach could retain each vehicle's autonomy while considering neighboring vehicles' objectives in the optimization. This improves scalability and possibly security compared to centralized control. All of these formulate the short-term OCP as a quadratic program and use a 10 s receding horizon [1].

6.1 Reference Trajectory

Each hierarchically-controlled vehicle begins by computing individualized state and control references $x_r = [s_r\ v_r\ a_r]^{\mathrm{T}}$ and u_r. With general PV position constraints delegated to the downstream RHC, the higher-level planner follows the speed-constrained solution of Section 4.3. First, the velocity reference $v_r(i)$ takes on the discretized result of (8a). Then, differentiation and integration of (8a) results in acceleration and position references $a_r(i)$ and $s_r(i)$, respectively. Finally, the omission of the first-order lag τ_a from OCP (3) to reduce model order necessitates an additional step to obtain $u_r(i)$. The first-order lag is therefore approximated as a one-step delay i.e. $u_r(i) = a_r(i+1)$ where the index i denotes the discrete step in the N-step prediction horizon. Different sampling times would require different numbers of delay steps to obtain matching performance.

6.2 Decentralized

The first hierarchical controller, termed Decentralized Hierarchical Control (DHC), considers the PV's trajectory as fixed and optimizes only the ego vehicle's control for its own objective in OCP (20). A quadratic cost penalizes state and control reference tracking errors $x_e = x - x_r$ and $u_e = u - u_r$.

$$\begin{aligned}
\min\ J = &x_e^{\mathrm{T}}(N)\,Px_e(N) + \sum_{i=0}^{N-1}\big[x_e^{\mathrm{T}}(i)\,Qx_e(i) \\
&\qquad\qquad\qquad + u_e^{\mathrm{T}}(i)\,Ru_e(i)\big] \\
\text{s.t.}\quad &\underline{u} \leq u(i) \leq \overline{u} \\
&u(i) - m_c v(i) \leq b_c, \quad i \in \{0,\ 1,\ \cdots\ N-1\} \\
&v(i) \geq 0 \\
&v(i) \leq \overline{v} \\
&a(i) \leq \overline{a} \\
&a(i) - m_c v(i) \leq b_c \\
&s(i) \leq s_p(i) - \underline{d}, \quad i \in \{1,\ \cdots\ N\}
\end{aligned} \tag{20}$$

Constraints prevent excessive or negative velocity, gaps less than $\underline{d}$ relative to the PV, and infeasible acceleration commands. The vehicle's maximal acceleration from the model described in Section 7.2 is simplified as a constant $\overline{u}$ that intersects with a line in (v, u) space with u-intercept b_c and negative slope m_c. Throughout this section, $\overline{v} = 30\,\mathrm{m/s}$ to allow the highest cycle speeds in Fig. 1. The linear model (1) links the inputs to the states.

[1] While Dollar and Vahidi (2018b) showed efficiency improvement with horizons longer than 10 s, Dollar and Vahidi (2018a) selected a 10 s horizon to limit computation time after lane decisions are introduced. Therefore, such a horizon is used here.

6.3 Centralized

In Centralized Hierarchical Control (CHC), the lead CAV receives individualized PMP-based plans from each vehicle in the string, then optimizes all m vehicles' control inputs to minimize collective deviation from these plans. The centralized OCP therefore uses combined state and input vectors $\mathcal{X}$ and $\mathcal{U}$, corresponding references $\mathcal{X}_r$ and $\mathcal{U}_r$, and a combined linear model. Recall the matrices A and B from the single-vehicle linear model (1) and let I_m denote the $m \times m$ identity matrix.

$$\mathcal{U} = \left[u_1 \ u_2 \ \cdots \ u_m\right]^{\mathrm{T}}, \quad \mathcal{X} = \left[x_1^{\mathrm{T}} \ x_2^{\mathrm{T}} \ \cdots \ x_m^{\mathrm{T}}\right]^{\mathrm{T}} \tag{21}$$

$$\mathcal{U}_r = \left[u_{r1} \ u_{r2} \ \cdots \ u_{rm}\right]^{\mathrm{T}}, \ \mathcal{X}_r = \left[x_{r1}^{\mathrm{T}} \ x_{r2}^{\mathrm{T}} \ \cdots \ x_{rm}^{\mathrm{T}}\right]^{\mathrm{T}} \tag{22}$$

$$\frac{d}{dt}\mathcal{X} = \left(\mathrm{I}_m \otimes A\right)\mathcal{X} + \left(\mathrm{I}_m \otimes B\right)\mathcal{U} \tag{23}$$

The objective is the unweighted sum of the individual objectives from (20), where $\mathcal{X}_e = \mathcal{X} - \mathcal{X}_r$ and $\mathcal{U}_e = \mathcal{U} - \mathcal{U}_r$. Let Ξ denote the feasible set of individual states x and control inputs u from (20), excluding the position constraint. In the centralized problem, only the lead CAV's position s_1 is constrained relative to the PV. The first constraint in (24a) also prevents CAVs from colliding with one another. In this and the following section, the subscript 0 denotes the PV i.e. $s_0 = s_p$.

$$\begin{aligned} \min \ \mathcal{J} = &\mathcal{X}_e^{\mathrm{T}}(N)\,\mathcal{P}\mathcal{X}_e(N) + \sum_{i=0}^{N-1}\left[\mathcal{X}_e^{\mathrm{T}}(i)\,\mathcal{Q}\mathcal{X}_e(i)\right. \\ &\left.+\mathcal{U}_e^{\mathrm{T}}(i)\,\mathcal{R}\mathcal{U}_e(i)\right] \\ \text{s.t.} \quad & s_j(i) \le s_{j-1}(i) - \underline{d} \\ & \{x_j, \ u_j\} \in \Xi \\ & i \in \{1, \ \cdots \ N\}, \ j \in \{1, \ \cdots \ m\} \end{aligned} \tag{24a}$$

$$\begin{gathered} \mathcal{P} = \mathrm{I}_m \otimes P, \quad \mathcal{Q} = \mathrm{I}_m \otimes Q \\ \mathcal{R} = \mathrm{I}_m \otimes R \end{gathered} \tag{24b}$$

The index j specifies a particular CAV, with j increasing from the front to the rear of the string. Note that the first position constraint involving s_0 only involves one decidable state because s_0 is considered fixed. The remaining position constraints each involve two decidable states.

After solving (24a), the lead CAV sends the optimal control inputs to the others in a master-slave scheme. Each slave vehicle applies the commanded control input ideally.

6.4 Cooperative

Equation (21) shows that the dimension of OCP (24a) increases with the number of agents in the string, which computationally limits the group's scale. A third hierarchical approach called Cooperative Hierarchical Control (CoHC) seeks most of centralization's benefit with improved scalability by only considering the ego and its immediate neighbors. In another distinction from master-slave CHC, each agent also determines its own control input. Impacts of the ego's control moves on its neighbors are modeled by adding the neighbors' moves as degrees of freedom but applying only the ego's result.

Agent q's group control and state vectors, references, and model are defined similarly to (21), (22), and (23) with only a subset $\mathcal{I}$ of vehicles included.

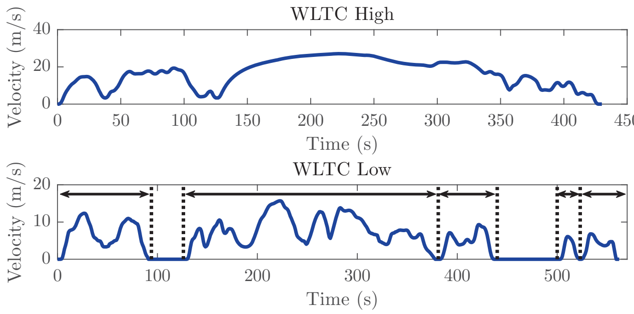

Fig. 1. The lead vehicle's drive cycles. The WLTC Low (bottom) is subdivided into the five segments demarcated with arrows.

$$\tilde{U} = \{u_w\}, \ w \in \left[\max\{1, \ q-1\}, \ \min\{q+1, \ m\}\right] \cap \mathbf{Z} \tag{25}$$

The cooperative objective is then identical to (24a) except that $\tilde{\mathcal{U}}$ and $\tilde{\mathcal{X}}$ replace $\mathcal{U}$ and $\mathcal{X}$. The vehicle indexing in the constraints is modified as follows. The future position of vehicle number $j = \max\{0, \ q-2\}$ is treated as fixed.

$$\mathcal{I} = \{j | j \in \{q-1, \ q, \ q+1\} \cap \{1, \ \cdots \ m\}\} \tag{26a}$$

$$\begin{aligned} &\{x_j, \ u_j\} \in \Xi \\ &s_j(i) \le s_{j-1}(i) - \underline{d} \\ &i \in \{1, \ \cdots \ N\}, \ j \in \mathcal{I} \end{aligned} \tag{26b}$$

Taking large m as an example, if $q = 1$ then CAVs 1 and 2 belong to $\mathcal{I}$, but if $q = 2$ then CAVs 1, 2, and 3 belong to $\mathcal{I}$. Although CAV 2 belongs to both sets, it applies only the u from its own optimization, that is, the $q = 2$ case.

7. SIMULATION METHODS

This section describes the scenarios and analysis by which the previously discussed algorithms are assessed.

7.1 Drive Cycle Disturbances

The common evaluation scenarios for all algorithms involve a string of 8 intelligent vehicles following an open-loop PV, which drives a known distance in a known time. Where applicable, these quantities determine $\overline{s}_{fd}$ and t_{fd}. The Worldwide Light-duty Test Cycle (WLTC) High and Low (World Forum for Harmonization of Vehicle Regulations (2015)) are evaluated, exposing the strings to different speeds and numbers of PV stops. Figure 1 shows the cycles' speeds over time.

In reality, intelligent driving cannot avoid all speed fluctuations. For example, stop signs require all vehicles to stop regardless of traffic. However, CAVs may attenuate other waves, such as temporary disturbances from cut-ins. To expose the controllers to both situations, full stops in the cycles are enforced for the string. This decouples the WLTC Low into five segments as shown in Figure 1.

7.2 Energy Assessment

A Nissan Leaf is modeled using publicly available data in order to compute the energy consumption for each simulation as previously described by Dollar et al. (2020). The process involves computing the motor speed ω_m and torque T_m from vehicle states, looking up the requisite

Table 1. Controller List

Controller	Acronym	Section
Adaptive Cruise, 0.8 s Headway	ACC, 0.8 s	3
Adaptive Cruise, 1.5 s Headway	ACC, 1.5 s	3
Position-Constrained Shrinking Horizon	PCSHC	5
Decentralized Hierarchical	DHC	6.2
Centralized Hierarchical	CHC	6.3
Cooperative Hierarchical	CoHC	6.4

motor power P_m, combining with auxiliary loads, and computing the total current to assess resistance losses. Newton's second law provides the traction force F_t considering resistance force coefficients a_v and c_v.

$$F_t = m_v a + a_v + c_v v^2 \tag{27}$$

A brake split model then apportions part of the total traction force F_t to the front-wheel-drive motor subject to the vehicle dynamics constraints described in Chu et al. (2011). The minimum traction force $\underline{F}_t < 0$ weakly depends on velocity.

$$F_f = \begin{cases} F_t & \frac{F_t}{\underline{F}_t(v)} \leq 0.04 \\ 0.73F_t + 0.0108\underline{F}_t(v) & \frac{F_t}{\underline{F}_t(v)} > 0.04 \end{cases} \tag{28}$$

The tire radius r_t and single drivetrain gear ratio r_g help determine the motor operating point. A constant drivetrain efficiency of $\eta_g = 0.95$ is assumed.

$$T_m = F_f \frac{r_t}{r_g} \eta_g^{-\mathrm{sgn} F_f}, \quad \omega_m = \frac{r_g}{r_t} v \tag{29}$$

A lookup table $P_m = f(\omega_m, T_m)$ maps the motor's speed and torque to its total power consumption, including motor and inverter losses, using data from Burress (2013). Losses in the battery with resistance R_b and open-circuit voltage V_0 are then computed via the battery current i_b. The analysis models the power electrical system as a combined motor and auxiliary power sink of value P_l in parallel with the battery. Only one of the two possible solutions to (30a) satisfies the battery current limit.

$$i_b = \frac{V_0(SOC) \pm \sqrt{V_0^2(SOC) - 4R_b P_l}}{2R_b} \tag{30a}$$

$$P_T = P_l + i_b^2 R_b = V_0(SOC)\, i_b \tag{30b}$$

All vehicles begin with a state-of-charge (SOC) of 60 %, from which point the total power P_T is integrated to find later SOC and cumulative energy consumption.

8. RESULTS

Because of its necessity for interpreting other results, this section begins with string stability. Next, the drive-cycle-disturbance results at both the single-vehicle and string levels are presented. Finally, the qualitative performance of the different algorithms is analyzed in detail to explain the differences in overall results. Table 1 lists the acronyms used for each algorithm.

8.1 String Stability

String stability has been defined in terms of range error (Liang and Peng (1999)) and disturbance attenuation (Gunter et al. (2019)) trends moving upstream in a string of vehicles. Since not all algorithms use a target position and disturbances cause excess acceleration, we examine mean acceleration to determine string stability. If the mean acceleration of a vehicle in response to a disturbance decreases as string index increases, we say that the controller is string stable. If the mean acceleration increases, we say that the controller is string unstable.

The classical ACC of Section 3 resulted in either string stability or instability depending on the choice of time headway as shown in Figure 2. The velocity-planned algorithms differ from the headway-based ACC in their immediate reduction of acceleration in the string's first follower. However, PCSHC resulted in string instability and by the end of the string, its acceleration exceeded that of the longer-headway ACC.

8.2 Cumulative Performance

Tables 2 and 3 list the first follower and string results for each algorithm, in order of improving string performance. The parabolic trajectory without a PV (Section 4.1) was also simulated as a high-performing benchmark. Although it would result in collisions, its performance marks the point beyond which further improvement is unlikely. Percent changes relative to the parabola reflect the impact of the position constraint; lower is better.

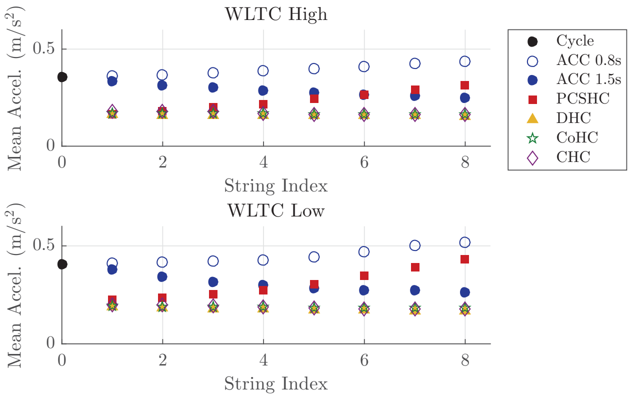

Fig. 2. Mean absolute acceleration from the front (lower index) to rear (higher index) of the string.

Table 2. WLTC High Results

Algorithm	First Follower		String	
	Energy MJ	% Diff.	Energy MJ	% Diff.
ACC, 0.8 s	3.728	10.7	30.120	11.8
PCSHC	3.504	4.1	29.598	9.9
ACC, 1.5 s	3.680	9.3	28.665	6.4
DHC	3.453	2.6	27.708	2.9
CoHC	3.463	2.9	27.672	2.7
CHC	3.465	2.9	27.649	2.7
Parabolic	3.367	-	26.934	-

Table 3. WLTC Low Results

Algorithm	First Follower		String	
	Energy MJ	% Diff.	Energy MJ	% Diff.
ACC, 0.8 s	1.155	29.5	9.416	32.0
PCSHC	0.949	6.4	8.301	16.4
ACC, 1.5 s	1.115	25.0	8.217	15.2
DHC	0.919	3.0	7.313	2.5
CoHC	0.917	2.8	7.298	2.3
CHC	0.907	1.7	7.173	0.6
Parabolic	0.892	-	7.133	-

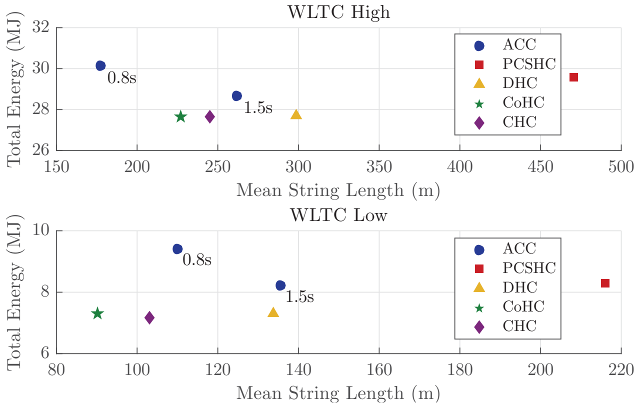

Fig. 3. Energy use and string length in WLTC High and Low cycles.

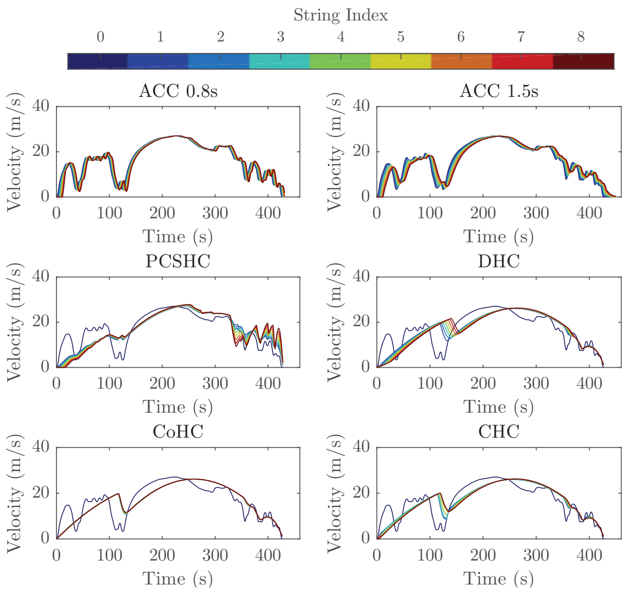

Fig. 4. Velocity trajectories in the WLTC High Cycle.

Considering the string, the hierarchical controllers performed best followed by string-stable ACC, PCSHC, and string-unstable ACC. However, PCSHC performed relatively well for the first vehicle. This underscores the importance of string evaluation to obtain a full view of control performance in traffic. In these scenarios, the hierarchical controllers' energy consumption approached that of the unconstrained parabolic trajectory with only a small improvement from collaboration. However, the more collaborative variants accomplished this energy performance in a more spacially-compact way as shown in Figure 3. This feature could translate into energy improvements in continuous traffic streams where throughput is critical.

In general, calibration of a given control system for a longer time headway improves energy efficiency and safety at the expense of string length. The two ACC calibrations shown in Figure 3 follow this expectation. The hierarchical algorithms move to the lower left of ACC using a combination of preview information and collaboration.

8.3 Qualitative Observations

Figures 4 and 5 show the velocity trajectories for the different algorithms. The ACC and PMP-based approaches

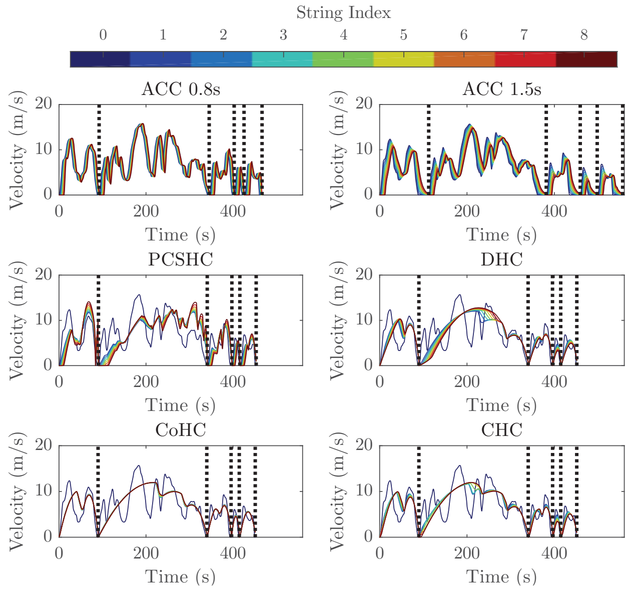

Fig. 5. Velocity trajectories in the WLTC Low Cycle.

clearly operate based on different principles. ACC targets a headway and thus forms a relatively compact string behind the PV as its cycle-like velocity traces show. In contrast, the PMP solutions target the final position and time, disregarding the PV unless it becomes an active constraint. This typically results in energy savings and compact CAV strings, but leaves large gaps between the PV and first CAV. Such approaches could be viable in single lane situations without busy side roads. However, in heavier multi-lane traffic they could invite cut-ins between the leader and first CAV. Collaboration helped the CAVs move as one, further compacting the CAV portion of the string. This phenomenon appears, for example, in the first 150 s of Figure 4. Notably, CoHC and CHC achieved lower average string length compared to the string-stable ACC without tracking a headway.

The PCSHC velocity trajectories reveal possible reasons for its lower string performance compared to other algorithms. Discontinuities appear in its acceleration mainly because of feasibility adjustments. Since a currently large negative a_p is assumed to persist in future, the controller tends to overreact to PV acceleration that is likely to fade or reverse after several seconds. Therefore, refinement of the future PV position function $s_p(\tau)$ and smoother feasibility adjustment may improve performance.

9. CONCLUSION

Five algorithms from three different families were evaluated for energy efficiency in the presence of a PV-related position constraint. Results generally trended as expected, with the connectivity-enabled optimal algorithms resulting in lower energy consumption compared to unconnected ones. The ACC controller was either string stable or unstable depending on time headway. Position-constrained shrinking-horizon control performed well for a single vehicle considering its lack of preview information, but was string unstable and displayed greater string energy consumption compared to stably-tuned ACC. Smoother feasibility adjustment and a stochastic PV position trajectory are promising areas for future PCSHC development.

Unexpectedly, this study found less than 2 % improvement in energy consumption from centralization. The main advantage of collaboration lay in string compactness, which generally indicates improved throughput in continuous traffic. These results suggest that decentralized control is sufficient for single-lane car following in light traffic. Such scenes might occur on rural single-lane roadways. Collaborative or centralized control could offer advantages in higher-demand situations like urban traffic jams.

ACKNOWLEDGEMENTS

R. A. D. thanks IFP Energies nouvelles for hosting him in France while this research was conducted.

REFERENCES

Bemporad, A., Bernardini, D., Long, R., and Verdejo, J. (2018). Model predictive control of turbocharged gasoline engines for mass production. In *WCX World Congress Experience*, 1–12. SAE.

Burress, T. (2013). Benchmarking state-of-the-art technologies. In *Oak Ridge National Laboratory, 2013 US DOE Hydrogen Fuel Cells Program Vehicle Technologies Program Annual Merit Review Peer Evaluation Meeting.*

Chu, L., Yao, L., Chen, J., Chao, L., Guo, J., Zhang, Y., and Liu, M. (2011). Integrative braking control system for electric vehicles. In *2011 IEEE Vehicle Power and Propulsion Conference*, 1–5. IEEE.

Dollar, R.A., Sciarretta, A., and Vahidi, A. (2020). Multi-agent control of lane-switching automated vehicles for energy efficiency. In *2020 American Control Conference*. IEEE. To appear.

Dollar, R.A. and Vahidi, A. (2018a). Predictively coordinated vehicle acceleration and lane selection using mixed integer programming. In *ASME 2018 Dynamic Systems and Control Conference*, V001T09A006–V001T09A006. American Society of Mechanical Engineers.

Dollar, R.A. and Vahidi, A. (2020). Automated driving with variational optimal control and mixed integer programming. *IEEE Transactions on Control Systems Technology*. In review.

Dollar, R.A. and Vahidi, A. (2018b). Efficient and collision-free anticipative cruise control in randomly mixed strings. *IEEE Transactions on Intelligent Vehicles*, 3(4), 439–452.

Gunter, G., Gloudemans, D., Stern, R.E., McQuade, S., Bhadani, R., Bunting, M., Monache, M.L.D., Lysecky, R., Seibold, B., Sprinkle, J., Piccoli, B., and Work, D.B. (2019). Are commercially implemented adaptive cruise control systems string stable? *arXiv preprint arXiv:1905.02108*, 1–22.

Han, J., Sciarretta, A., Ojeda, L.L., De Nunzio, G., and Thibault, L. (2018). Safe-and eco-driving control for connected and automated electric vehicles using analytical state-constrained optimal solution. *IEEE Transactions on Intelligent Vehicles*, 3(2), 163–172.

Han, J., Vahidi, A., and Sciarretta, A. (2019). Fundamentals of energy efficient driving for combustion engine and electric vehicles: An optimal control perspective. *Automatica*, 103, 558–572.

He, C.R., Ge, J.I., and Orosz, G. (2019). Fuel efficient connected cruise control for heavy-duty trucks in real traffic. *IEEE Transactions on Control Systems Technology (Early Access)*, 1–8. doi:10.1109/TCST.2019.2925583.

Kim, N., Cha, S., and Peng, H. (2010). Optimal control of hybrid electric vehicles based on Pontryagin's minimum principle. *IEEE Transactions on Control Systems Technology*, 19(5), 1279–1287.

Kim, Y., Guanetti, J., and Borelli, F. (2019). Robust eco adaptive cruise control for cooperative vehicles. In *18th European Control Conference (ECC)*, 1214–1219. IEEE.

Liang, C.Y. and Peng, H. (1999). Optimal adaptive cruise control with guaranteed string stability. *Vehicle System Dynamics*, 32(4-5), 313–330.

Milanés, V. and Shladover, S.E. (2014). Modeling cooperative and autonomous adaptive cruise control dynamic responses using experimental data. *Transportation Research Part C: Emerging Technologies*, 48, 285–300.

Ntousakis, I.A., Nikolos, I.K., and Papageorgiou, M. (2015). On microscopic modelling of adaptive cruise control systems. In *4th International Symposium of Transport Simulation*, 111–127. Transportation Research Procedia.

Paredes, J.F., Cazar, G.P., and Donkers, M. (2019). A shrinking horizon approach to eco-driving for electric city buses: Implementation and experimental results. *IFAC-PapersOnLine*, 52(5), 556–561.

Sciarretta, A. and Vahidi, A. (2019). *Energy-Efficient Driving of Road Vehicles: Toward Cooperative, Connected, and Automated Mobility*. Springer.

Shladover, S.E., Su, D., and Lu, X.Y. (2012). Impacts of cooperative adaptive cruise control on freeway traffic flow. *Transportation Research Record*, 2324(1), 63–70.

Vahidi, A. and Eskandarian, A. (2003). Research advances in intelligent collision avoidance and adaptive cruise control. *IEEE Transactions on Intelligent Transportation Systems*, 4(3), 143–153.

World Forum for Harmonization of Vehicle Regulations (2015). Proposal for amendments to global technical regulation no. 15 on worldwide harmonized light vehicles test procedure. Technical Report ECE/TRANS/WP.29/GRPE/2016/3, United Nations, Geneva.

Xiao, L. and Gao, F. (2010). A comprehensive review of the development of adaptive cruise control systems. *Vehicle System Dynamics*, 48(10), 1167–1192.